

Physics-Based Dynamic Models Hybridisation Using Physics-Informed Neural Networks

¹Branislava Lalic*, ²Dinh Viet Cuong*, ³Mina Petric, ⁴Vladimir Pavlovic, ¹Ana Firanj Sremac, ⁵Mark Roantree

¹Faculty of Agriculture, University of Novi Sad, Novi Sad, Serbia

²School of Computing, Dublin City University, Dublin 9, Ireland

³AVIA GIS, Zoersel, Belgium

⁴Department of Computer Science, Rutgers University, New Brunswick, NJ, USA

⁵Insight Centre for Data Analytics, Dublin City University, Dublin 9, Ireland

Physics-based dynamic models (PBDMs) are simplified representations of complex dynamical systems. PBDMs take specific processes within a complex system and assign a fragment of variables and an accompanying set of parameters to depict the processes. As this often leads to suboptimal parameterisation of the system, a key challenge requires refining the empirical parameters and variables to reduce uncertainties while maintaining the model's explainability and enhancing its predictive accuracy. We demonstrate that a hybrid mosquito population dynamics model, which integrates a PBDM with Physics-Informed Neural Networks (PINN), retains the explainability of the PBDM by incorporating the PINN-learned model parameters in place of its empirical counterparts. Specifically, we address the limitations of traditional PBDMs by modelling the parameters of larva and pupa development rates using a PINN that encodes complex, learned interactions of air temperature, precipitation and humidity. Our results demonstrate improved mosquito population simulations including the difficult-to-predict mosquito population peaks. This opens the possibility of hybridisation concept application on other complex systems based on PBDMs such as cancer growth to address the challenges posed by scarce and noisy data, and to numerical weather prediction and climate modelling to overcome the gap between physics-based and data-driven weather prediction models.

Keywords: hybridisation, physics-based dynamic models, physics-informed neural networks (PINN), hybrid dynamic model, mosquito population modelling

1 Introduction

Physics-based dynamic models (PBDMs) are widely used in research and technology, from predicting air temperature to modelling COVID-19 spread and cancer cell development. As Willcox et al. (2021) [1], citing Wigner (1960) [2], highlighted, "... physics-based modelling is powerful and effective because it gives us a predictive window into the future based on understanding". It achieves this because any specific model limits its scope to a particular class of physical systems or processes, building a universal representation within that class.

However, there remains a gap between the PBDMs developed to better understand and simulate a class of systems or processes and their ability to accurately simulate individual system behaviours using available data. Bridging this gap requires increased level of detail and data about the particular system to compensate for initial simplifications. Achieving these objectives requires comprehensive **data collection** and the **extraction of meaningful insights** from it.

According to Statista (2022) [3] - "The total amount of data created, captured, copied, and consumed globally is forecast to increase rapidly, reaching 64.2 zettabytes in 2020 and by 2025, global data creation is projected to grow to more than 180 zettabytes". Despite the exponential growth in data creation, our ability to assimilate and understand this data lags significantly behind.

The increase in data volume and the capacity of artificial intelligence communities to develop predictive models are not, even closely, proportional to our ability to **extract knowledge from data** by applying an inverse problem theory in the broadest possible sense, as it was perfectly brought by Wilcox et all. (2021) [1] ("In general, any endeavor to infer cause from effect — to extract knowledge from data — can be viewed as an inverse problem") and to **extract data from knowledge** by developing models that, while still physics-based, learn more from data with the capacity for extrapolation beyond limits of observed data.

Our answer to this challenge is **the deep fusion between physics and artificial intelligence (AI)**. For decades, these two scientific disciplines have been considered as parallel approaches to the problem-solving future. Physics-based and AI models are generally deployed as separate, parallel solutions, where scientists implement one or the other approach. We reject this *either-or* concept and instead believe that only synergies of the two concepts can accelerate research and innovation for many complex tasks.

Having only recently come to light [1,4,5], the hybrid dynamic model approach is still at the level of reviews and recommendations. Our design of **hybrid physics-based dynamic models** is based on the *tight* coupling of physics-based and AI models "to process large and rapidly increasing amounts of data to provide more accurate, less uncertain, and physically consistent inferences in the form of prediction, modelling and understanding" [4] the complex dynamic processes. This coupling will be achieved by the hybridization of PBDMs with AI models such as Physics-Informed Neural Networks (PINNs) and Physics-Guided Neural Networks (PGNNs). The objective is to enhance the capabilities and accuracy of PBDMs by strategically incorporating machine learning at critical points within existing physics-based models, thereby producing advanced **hybrid dynamical models (HyDM)**.

The fast emerging (3,937 published papers since 2018 and 2,174 preprints, according to SCOPUS) Physics-Informed Neural Networks (PINN) are making first steps into the realm of physics-based models, aiming to replace some fundamental elements of dynamic models, such as differencing methods [6] and parameterisations of basic processes [7], while still facing challenges related to fundamental principles like mass conservation [8]. While PINNs have made notable advancements in integrating physics and AI, they primarily address aspects of parameterisation and differential equation solutions. Our approach extends this line of research by anticipating the strategic incorporation of machine learning at key points within existing PBDMs. By doing so, we aim to create more flexible, dynamic models that are capable of adapting to diverse real-time scenarios.

In this paper, we explore the potential of hybrid models to bridge the gap between traditional PBDMs and the complex, real-time behaviour of specific systems. This approach allows us to not only improve predictive capabilities but also reduce uncertainties associated with traditional models. We present our conceptual design and provide an example of a **HyDM** implementation through an inverse problem application in dynamical modelling using PINNs.

2. Methodology

2.1 The concept of physics-based dynamic model hybridisation

The leverage points of a dynamic model are the model's parameters, functions or components where minor changes can lead to significant changes in model simulations [9]. One of the primary tasks in model hybridisation is to identify model leverage points and test their consistency with leverage points of actual system. We have identified several model elements and features as potential key points where AI can be integrated into physical models. While this paper focuses on improving the model's predictive capability through PINN integration, we outline these key points as part of a broader conceptual framework. Although not all of these areas will be addressed in our current study, they serve as important overview of opportunities for hybridization of PBDMs with AI in the future.

These key leverage points include:

- a) *Physical model.* Constitutive and conservation laws form the backbone of every PBDMs, aiming to interpret physical, biological, or chemical processes of interest. However, as the system deviates from homogeneous and isotropic, the representative power of the modelled processes and the empirical parameterisations become increasingly uncertain. The selection of a representative physical model and determination of parameters are **par excellence inverse problems**, and Physics-Informed Neural Networks (PINNs) offer a potentially powerful solution, particularly in cases of scarce data.
- b) *Forcing.* Accurately determining internal and external factors that affect system state over time is crucial for the reliability and accuracy of model predictions. Data-driven forcing determination based on historical data enables the identification of new or improved parameterisation of already identified, forcing factors and system responses. Identification of forcing factors and models is an active area of research at the intersection of physical modelling and machine learning, extending into concepts of attribution and general causality [10-12].
- c) *Initial conditions.* The system's initial state (independent variable values at the start of integration) results from its history and is typically very difficult to determine. Newly available database and AI tools to manage initial conditions can enable new insights into initial conditions of dynamical systems. If the state of the external system affects system dynamics, initial condition problem solving can be extended to boundary condition using the same methodology [13-15].
- d) *Bias.* Understanding and reducing deviations of simulated values from observations (bias) will come from complex patterns of time series bias and their correlation with initial conditions and forcing data. Hybridisation of physical & deep models opens the possibility

for simultaneous reduction of the modelling risk (bias + variance) with complex deep model structures [16,17].

- e) *Uncertainties.* A broad range of external factors can affect system behaviour under specific circumstances, even if these factors were not considered during the modelling process. These external factors introduce epistemic uncertainties in the system's behaviour. Identification and quantification of these uncertainties, as well as those introduced by the aleatoric uncertainties in the data, is essential [18] and can be, for instance, performed using a PINN trained with external forcing signals, such as the weather data in addition to the ODE input data.

2.2 Inverse problem application

The **HyDM** used in this study was developed using Physics-Informed Neural Networks (PINN), presented in Cuong et al. (2024) [19], to apply inverse theory, evaluate, and refine ground parameterisations and empirical sub-modules of a physics-based dynamic model.

Dynamic model (Dy_PopMosq). We selected the population dynamics model (Dy_PopMosq) developed by Petric (2020) [20] as a hybridisation case study. The mosquito life cycle is divided into 10 stages: egg (E), larva (L), pupa (P), emerging adults (A_{em}), nulliparous bloodseeking adults (A_{b1}), nulliparous gestating adults (A_{g1}), nulliparous ovipositing adults (A_{o1}), parous bloodseeking adults (A_{b2}), parous gestating adults (A_{g2}) and parous ovipositing adults (A_{o2}). The dynamical system is expressed in equation (1) as a full ODE system

$$\left\{ \begin{array}{l} \frac{dE}{dt} = \gamma_{Ao}(\beta_1 A_{o1} + \beta_2 A_{o2}) - (\mu_E + f_E)E \\ \frac{dL}{dt} = f_E E - \left(m_L \left(1 + \frac{L}{\kappa_L} \right) + f_L \right) L \\ \frac{dP}{dt} = f_L L - (m_P + f_P)P \\ \frac{dA_{em}}{dt} = f_P \sigma e^{-\mu_{em} \left(1 + \frac{1}{\kappa_P} \right)} P - (m_A + \gamma_{Aem}) A_{em} \\ \frac{dA_{b1}}{dt} = \gamma_{em} A_{em} - (m_A + \mu_r + \gamma_{Ab}) A_{b1} \\ \frac{dA_{g1}}{dt} = \gamma_{Ab} A_{b1} - (m_A + f_{Ag}) A_{g1} \\ \frac{dA_{o1}}{dt} = f_{Ag} A_{g1} - (m_A + \mu_r + \gamma_{Ao}) A_{o1} \\ \frac{dA_{b2}}{dt} = \gamma_{Ao} (A_{o1} + A_{o2}) - (m_A + \mu_r + \gamma_{Ab}) A_{b2} \\ \frac{dA_{g2}}{dt} = \gamma_{Ab} A_{b2} - (m_A + f_{Ag}) A_{g2} \\ \frac{dA_{o2}}{dt} = f_{Ag} A_{g2} - (m_A + \mu_r + \gamma_{Ao}) A_{o2} \end{array} \right. \quad (1)$$

where the parameters are explained in the Table SA1 in Supplementary A. These parameters are determined from observations and laboratory experiments and considered a baseline for this research [20-25]. Air temperature is considered as the main forcing factor in Dy_PopMosq. Initial conditions are set to 300 for all stages and the model spin up time is estimated at approximately 200 days [26]. Bias reduction is not applied in the original model.

Physics-Informed Neural Network (PINN_PopMosq). PINN_PopMosq was developed based on the PINN model presented in Cuong et al. (2024) [19], which used only idealised annual variations of daily temperature as input meteorological conditions. However, based on our knowledge about mosquito population development, we anticipated that not only air temperature, but also air humidity and precipitation play active roles of “forces” affecting our biological system. To incorporate a complete set of measured meteorological data, we introduce a novel aspect by employing parameter networks that accept inputs from meteorological conditions. Additionally, we propose the use of a Multi-branch Fourier-feature Multi-Layer Perceptron (FourierMLP) for the parameter networks to enhance generalisation capabilities. Furthermore, we implement a modified absolute activation function to enforce parameter positivity.

Let $u(t) = (E(t), L(t), P(t), A_{em}(t), A_{b1}(t), A_{g1}(t), A_{o1}(t), A_{b2}(t), A_{g2}(t), A_{o2}(t)) \in \mathbb{R}^{10}$ represent the state of the mosquito dynamical system at time t , where each element of u corresponds to the population count of a specific life stage in the mosquito life cycle. Let $a(t)$ denote the vector of meteorological conditions at time t , and let θ denote the system parameter(s) defined in equation (1), influenced by these conditions.

We are given a set of observations $\mathcal{D}_u = \{(t_1, u_1), (t_2, u_2), \dots, (t_j, u_j), \dots\}$. The observations may not contain a full state as only some elements of state are observed. Assume we have a trained function $A: t \mapsto A(t)$ that approximates the meteorological variables with reasonable accuracy. The objective is to learn a mapping from the meteorological variables a to the system parameters θ such that the resulting state u not only aligns with the observed data \mathcal{D}_u but also satisfies the ODE system described in equation (1). This approach aims to integrate data-driven learning with the underlying physical principles represented by the ODEs.

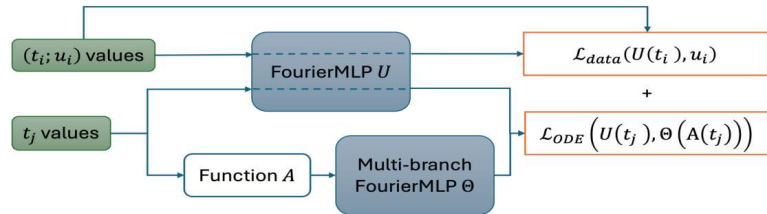


Figure 1 PINN Framework.

We adopt a PINN approach, which follows the framework presented in Figure 1, and inspired by [19, 27]. Specifically, the state function u is approximated by a neural network U that maps time t to the estimated state $u(t)$. Concurrently, each unknown parameter is represented by a neural network that takes $A(t)$ values as inputs and produces the corresponding parameter values. We denote the system parameters, either known or replaced by neural networks, by θ and refer to them as neural networks. The neural networks U and θ are parameterised by W_U and W_θ which are jointly optimised to minimise the objective function captured in equations (2)-(4).

$$\mathcal{L} = \mathcal{L}_{data} + \mathcal{L}_{ODE} = \mathcal{L}_{data} + \frac{1}{F} \sum_{i=1}^F \lambda_i \mathcal{L}_{f^{(i)}}, \quad (2)$$

with

$$\mathcal{L}_{data} = \frac{1}{N_u} \sum_{(t_i, u_i) \in \mathcal{D}_u} (U(t_i) - u_i)^2 \quad (3)$$

$$\mathcal{L}_{f^{(i)}} = \frac{1}{N_f} \sum_j \left| \frac{dU}{dt} - f^{(i)}(t_j, U(t_j), \theta(A(t_j))) \right|^2. \quad (4)$$

Here, $f^{(i)}, i = 1, \dots, 10$, denote the ten ODEs presented in equation (1); λ_i are weights that balance the multiple objectives within the loss function; N_u denotes the number of state observations; while N_f represents the number of collocation points t_j randomly sampled from the interval $[0, T]$. When the state is not fully observed, unavailable entries are masked out in the loss \mathcal{L}_{data} .

The objective function comprises two components: \mathcal{L}_{data} which ensures that the predictions made by the model U closely align with the observed data, and $\mathcal{L}_{f^{(i)}}$ which minimises the ODE residuals. By optimising these terms simultaneously, we aim to learn a system state and parameter set that not only fits the real-world observations but also satisfies the underlying ODE system.

For the neural network architectures of U, Θ and possibly A , we implement FourierMLP [28], which has demonstrated significant improvements in both convergence speed and accuracy for PINN training [29].

Given an input x to the neural network FourierMLP, the output y is defined in equation (5).

$$\begin{aligned} h^{(0)} &= [\cos(Bx); \cos(Bx)] \\ h^{(l)} &= \phi_h(W^{(l)}h^{(l-1)} + b^{(l)}), l = 1, \dots, L-1 \\ y &= \phi_o(W^{(L)}h^{(L-1)} + b^{(L)}) \end{aligned} \quad (5)$$

where B is a random matrix with entries sampled from a normal distribution $\mathcal{N}(0, \sigma)$. $W^{(l)}$ and $b^{(l)}$ represent the weights and biases of appropriate dimensions, respectively. During the training process, B remains fixed while the weights and biases are optimised. L denotes the number of hidden layers, and ϕ_h is the element-wise activation function applied to the hidden layers.

We employ the Gaussian Error Linear Unit (GeLU) activation function [30] for ϕ_h , as it provides a smooth non-linearity to the model.

To enforce non-negativity constraints on the state or parameters, we propose a soft absolute function as the output activation function ϕ_o shown in equation (6) where ϵ is determined to be 10^{-4} through experimentation.

$$\phi_o(x) = \sqrt{x^2 + \epsilon} - \sqrt{\epsilon}, x \in \mathbb{R} \quad (6)$$

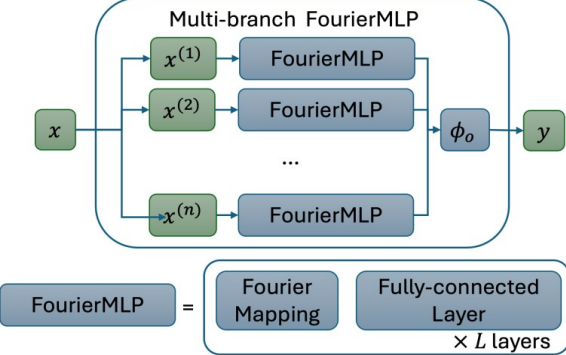


Figure 2 Multi-branch Fourier-MLP PINN Framework.

The meteorological variables $A(t)$ typically originate from a high-dimensional space, while the available training data is often limited. This frequently leads to poor generalisation of trained models. Therefore, we propose a multi-branch architecture for the external-to-parameter networks Θ , as illustrated in Figure 2. Our proposed architecture comprises multiple branches (n branches are depicted in Figure 2), each consisting of a separate FourierMLP that processes a distinct group of inputs. The outputs from these branches are subsequently combined in later layers to produce the final prediction.

Formally, let us consider n groups of external factors represented by vectors $x^{(1)}, \dots, x^{(n)}$.

Each input vector $x^{(i)}$ is processed by a dedicated branch FourierMLP $^{(i)}$. The outputs from these branches are then aggregated through summation and passed through a final activation function ϕ_o , as described by the following equation:

$$y = \phi_o(\sum_i \text{FourierMLP}^{(i)}(x^{(i)})) \quad (7)$$

We employ the gradient-based Adam optimizer [31] to minimise the objective functions discussed earlier. All differentiation operations, including derivatives in the ODE equations and optimisation gradients, are computed using automatic differentiation provided by the PyTorch framework [32]. To enhance convergence and accuracy, we implement ODE normalisation and gradient balancing techniques as proposed in Cuong et al. (2024) [19]. ODE normalisation rescales the inputs and outputs of the neural networks and reformulates the loss function to ensure that these quantities remain within reasonable ranges. Gradient balancing adaptively adjusts the weights λ_i throughout the training process to maintain balance across tasks when optimising multiple objectives simultaneously. Furthermore, we resample the collocation points for ODE residual calculations at each training step from a uniform distribution over the time domain. To facilitate convergence, we initially train the networks using only the data loss, allowing the network U to capture the general solution shape before moving onto satisfying both objectives. Finally, we train a separate FourierMLP to approximate meteorological data, providing a continuous function A for the framework. This neural network is frozen during the PINN training process, serving as a fixed input to the main model.

Hybrid PopMosq model (Hy_PopMosq). Evaluation of model ground parameterisations (Supplementary B, Fig. SB1) shows that the pupa development rate, f_P (or larva development rate $f_L = 1.65f_P$), is the key leverage point of the Dy_PopMosq model, exerting the greatest influence on

the number of adults, both female and male ($A_{b1} + A_{b2}$). These results are consistent with entomological findings, which recognize pupa and larva development rates as critical factors influencing population growth dynamics [33,34]. Therefore, we select f_P as the system parameter to be learned by the PINN model from meteorological measurements and entomological observations. Once learned, this parameter will replace empirical formulas in the Dy_PopMosq ODE system, creating the hybrid Hy_PopMosq model.

A custom-designed numerical experiment was created to address the key features of mosquito population dynamics: the timing and intensity of population (number of adults) growth, as well as the timing of population local peaks (temporary surge in population time series), which is, from the point of protective measures application, the most important population time series characteristic.

In addition to analysing the normalised model outputs, equal focus is given to its first derivative which indicates the rate of change. The timing of population peaks is also examined thoroughly. The integration time step is set to one day, based on the meteorological **forcing** data. **The initial conditions** are predefined only for the first year using the same initial conditions learnt by the neural network U in training data. For each subsequent year, the simulated values at the end of the previous year are used as initial conditions for the following year's simulations, ensuring the continuity condition of the population time series. Details of the numerical experiment design can be found in Supplementary C.

2.3 Data

Data used for training PINN_PopMosq are obtained from a two-year experiment conducted at a semi-urban location in Petrovaradin (Serbia) during 2016 and 2017. Daily mosquito trap counts were recorded alongside meteorological measurements, including daily air temperature (average, maximum, minimum), relative humidity (average), and precipitation. The comparison study uses daily meteorological data to run both the Dy_PopMosq and Hy_PopMosq models for the period of 2000-2007. Model validation is based on daily mosquito trap counts at the same location, conducted once per week (referred to as weekly catches) during 2000-2007 period. As meteorological measurements were not conducted on-site during this time, data from 2016 and 2017 for Petrovaradin and the Rimski Sancevi (Serbia) climate station were used to create a linear regression model, which estimates values at the Petrovaradin location based on available Rimski Sancevi climate station data.

2.4 Validation methodology

Performance metrics used in the study are: a) root-mean-square-error (RMSE) and standard deviations of the simulated and observed (σ_o) normalised population, along with their first derivatives; and b) peak prediction metrics that includes recall (percentage of observed peaks that are correctly predicted), precision (percentage of predicted peaks that match the observed peaks), and f1-score (harmonic average of recall and precision). The model is considered superior if, for normalised population values and their first derivatives, a) the RMSE is smaller; and b) following Pielke (1984), the RMSE is less than the standard deviation of observed values (σ_o), and the standard deviation of the simulations closely matches the standard deviation of the observed values (σ_o). This combination of error minimisation (through RMSE) and variability matching (through σ comparison), helps to ensure both accuracy and reliability in the model's performance. When one model produces

RMSE values smaller than σ_o , while the σ of the simulated data is closer to σ_o for another model, we do not immediately conclude which model is better. Instead, we revisit both the observed and simulated data to investigate why simulations may have, for example, a smaller RMSE but larger value for σ .

3 Results and Discussion

The comparison of Hy_PopMosq and Dy_PopMosq models, based on the performance metrics (Tabs. 1 and SD1) and the simulated and observed values of adult mosquito population (Fig. 3), as well as rate of adult mosquito population growth (Fig. 4), offers important insights into model strengths and weaknesses in simulating mosquito population dynamics. Both models are evaluated using outlined performance metrics and criteria (Sec. 2.4), focusing on error minimisation and variability matching. This analysis highlights the distinctive behaviour of models over the integration period that includes eight years, paying special attention to 2002 and 2007, where both models exhibited notable deviation from observed values. One of key findings is that Hy_PopMosq generally outperforms Dy_PopMosq in terms of population RMSE, achieving an overall lower RMSE (0.18 on average compared to 0.26 for Dy_PopMosq), which is not lower than σ_o but is closer to this threshold in comparison to Dy_PopMosq. The lower RMSE values are found across all years (Table SD1), including the outlier years 2002 and 2007, when the observed population peaks contribute to high RMSE values for both models. The peak in June 2002 (Fig. 3) exceeds typical counts of adult mosquitoes, suggesting that environmental factors outside of meteorological conditions (pond retention after heavy rain or even water pipe burst, for example) significantly affected population dynamics. Despite these deviations, Hy_PopMosq performs better in terms of capturing the population trends and maintaining a better alignment with observed data.

When comparing the models' ability to match observed population variability, Hy_PopMosq proves to be closer to the standard deviation of observed values ($\sigma = 0.12$) than Dy_PopMosq ($\sigma = 0.16$), further supporting its superiority in matching population fluctuations.

In simulating population growth rates (Fig. 4), Hy_PopMosq once again demonstrates a stronger overall performance with an average growth rate RMSE of 0.17 compared to 0.21 for Dy_PopMosq and standard deviation of observed population growth rate of 0.16 (Tabs. 1 and SD1). This indicates that Hy_PopMosq is more accurate in simulating the rate of change in mosquito populations. However, both models have difficulties in replicating the sharp population changes registered in 2007, indicating that there are still limitations in both models' capacity to capture rapid shifts in population dynamics. Additionally, when analyzing the growth rate variability, Dy_PopMosq exhibits a slight advantage ($\sigma_{rate} = 0.12$) over Hy_PopMosq ($\sigma_{rate} = 0.10$), but not enough to affect our determination regarding model superiority.

An additional insight emerges when excluding the two worst-performing years, 2002 and 2007, from the analysis. When these years are removed from the performance metrics, Hy_PopMosq's performance shows a more substantial improvement than Dy_PopMosq's performance, as demonstrated by the values in brackets in Table 1. This indicates Hy_PopMosq's robustness and ability to handle typical population dynamics better than Dy_PopMosq, which struggles with both extreme and normal conditions.

Peak detection is another element in which Hy_PopMosq outperforms Dy_PopMosq. The Hy_PopMosq model achieves a higher peak recall (0.56) and precision (0.63), leading to an F1 score of 0.57, which is significantly better than Dy_PopMosq's performance, where peak recall (0.13) and precision (0.09) are much lower. Figure 3 visually supports the findings, showing that Hy_PopMosq more closely aligns with the peaks in the observed adult population compared to Dy_PopMosq.

This indicates that enhanced parameterisation of other development rates can lead to more accurate simulations of mosquito population dynamics and peak predictions. It is important to notice that beyond the commonly used average daily air temperature, the PINN model used a full set of meteorological data during the learning process. Furthermore, both models demonstrated numerical stability. Although determining initial conditions based on the end-of-previous year's results is physically realistic, it carries the risk of error propagation in long-term simulations.

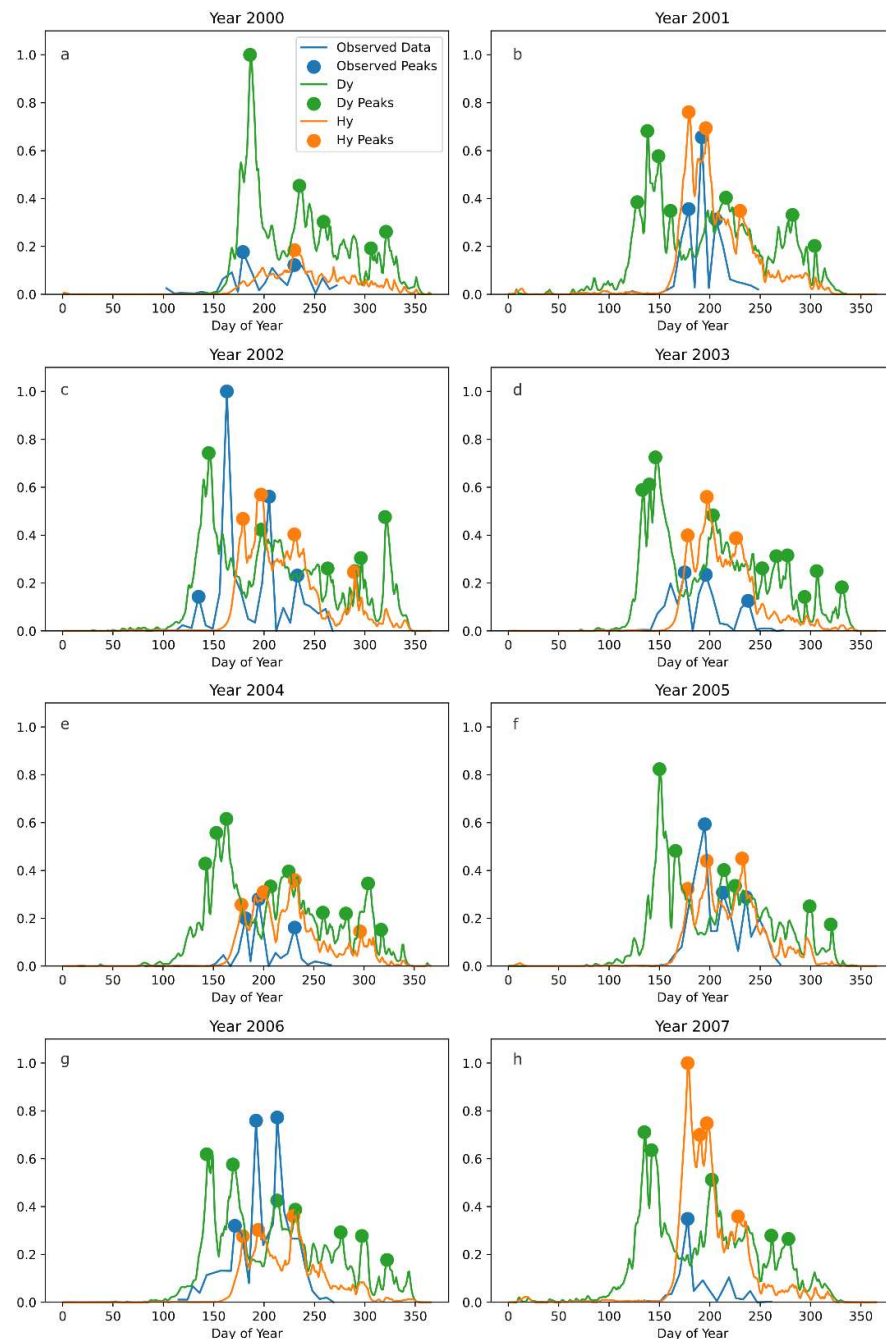


Figure 3 Adult mosquito population simulations ($A_{b1}+A_{b2}$).

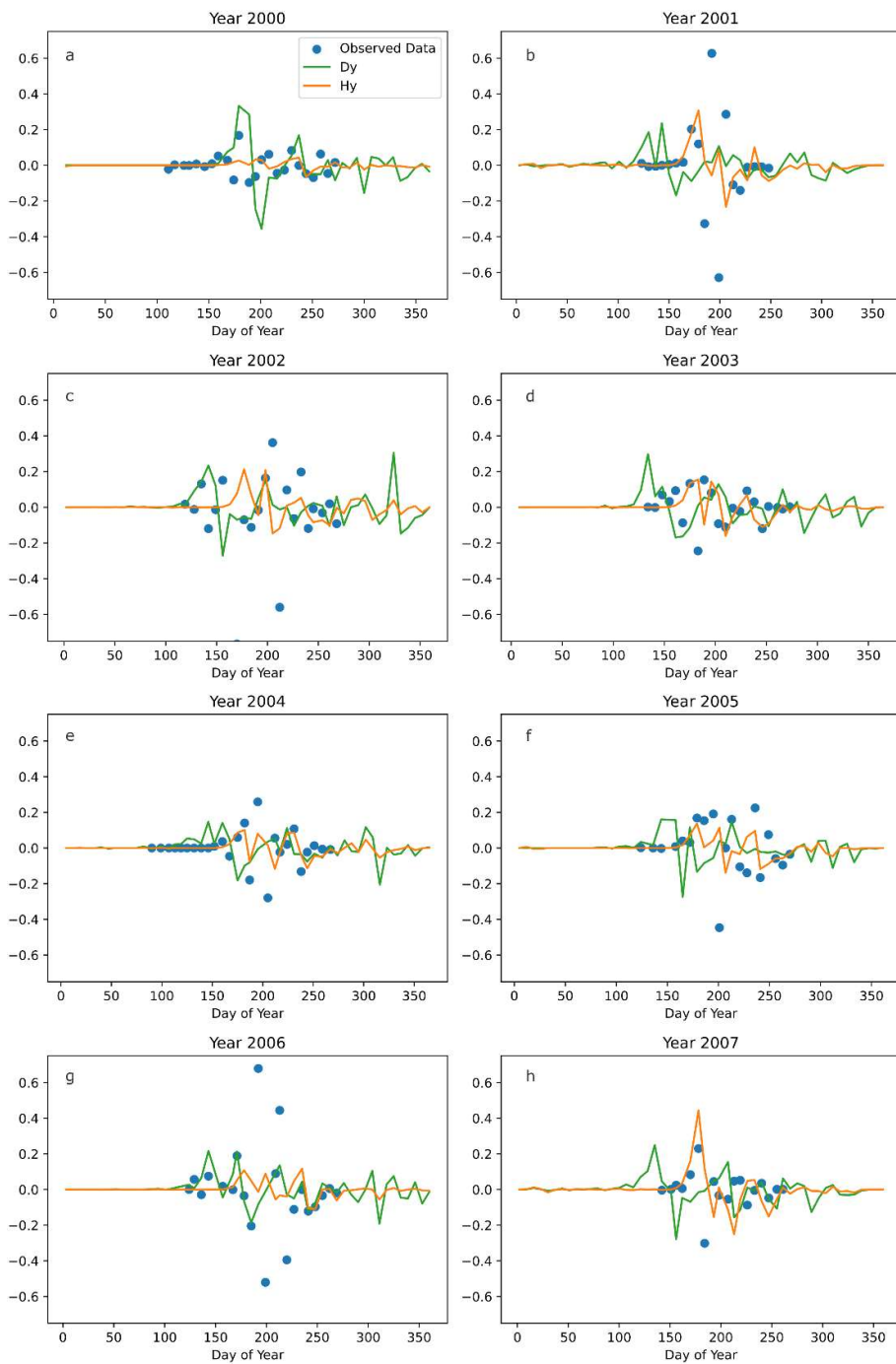


Figure 4 Rate of adult mosquito population growth.

	Dy_PopMosq	Hy_PopMosq	Observed
RMSE_population	0.26 (0.25)	0.18 (0.14)	-
$\sigma_{\text{population}}$	0.16	0.12	0.13
RMSE_rate	0.21 (0.17)	0.17(0.14)	-
σ_{rate}	0.12	0.10	0.16
No. Peaks	3.63	1.38	1.88
Peak recall	0.13	0.56	
Precision Peak	0.09	0.63	
F1 Peak	0.11	0.57	

Table 1 Performance metrics for Dy_PopMosq and Hy_PopMosq. Values in brackets refer to performance metrics when two worst-performing years are removed.

Conclusions

According to the results obtained in this study, Hy_PopMosq is consistently the superior model, particularly in terms of detecting population peaks, maintaining lower RMSE and matching variability of observed population. Both models however, face difficulties in the case of extreme variations of adults population, pointing to the need for further improvement and the incorporation of additional, environmental variables that may account for such deviations.

The hybridisation of the Dy_PopMosq model through enhanced parameterisation of pupa and larva development rates has led to significant improvements in modelling mosquito population dynamics. Additionally, through improved parameterisation of biological processes using PINN-learned empirical parameters, we gathered additional knowledge regarding the impact of meteorological elements other than temperature on larva and pupa development.

Further research will proceed in two primary directions.

The first direction involves testing the capability of Hy_PopMosq to improve other aspects of biological process modelling by incorporating a broader spectra of meteorological and non-meteorological parameters. These parameters are known or suspected to influence mosquito population dynamics but have not yet been explicitly accounted for in the parameterisations. Additional efforts will focus on better presentation of external forces affecting the system, improving initial conditions, reducing bias and uncertainties, and assessing the model's ability to integrate memory of introduced dynamical processes.

The second direction will test the hybridisation concept on other dynamical systems such as agricultural pest populations where successful practices from mosquito modelling can be applied. We will also apply this work to cancer growth, where hybridisation may address challenges posed by scarce and noisy data as well as the complexity of the growth processes. Finally, in atmospheric modelling, the application of hybridisation in numerical weather prediction and climate modelling can help to bridge the gap between physics-based (GFS, WRF, for example) and data-driven (GraphCast, FourCastNet, for example) weather forecast models.

This research demonstrates the power of transdisciplinary collaboration among physicists, meteorologists, entomologists, and AI researchers, highlighting that future breakthroughs across diverse fields have the best chance of success through integrated efforts such as these.

Data availability

The datasets generated during and/or analysed during the current study are available in the GitHub repository, <https://github.com/dinhvietcuong1996/external-pinn-mosquito>.

Code Availability

The code used for generating and analysing the data during the current study is available from the corresponding author upon reasonable request.

References

- [1] Willcox, K. E., Ghattas, O. & Heimbach, P. The imperative of physics-based modeling and inverse theory in computational science. *Nat. Comput. Sci.* **1**, 166–168 (2021).
- [2] Wigner, E. P. The unreasonable effectiveness of mathematics in the natural sciences. Richard courant lecture in mathematical sciences delivered at New York University, May 11, 1959. *Comm. Pure. Appl. Math.* **13**, 1–14 (1960).
- [3] Statista. <https://www.statista.com/statistics/871513/worldwide-data-created/> (2022).
- [4] Reichstein, M. *et al.* Deep learning and process understanding for data-driven Earth system science. *Nature* **566**, 195–204 (2019).
- [5] Molina, M. J. *et al.* A Review of Recent and Emerging Machine Learning Applications for Climate Variability and Weather Phenomena. *Artificial Intelligence for the Earth Systems* **2**, 220086 (2023). <https://doi.org/10.1175/AIES-D-22-0086.1>
- [6] Lu, K., Su, Y., Bi, Z., Qiu, C. & Zhang, W. Characteristic Performance Study on Solving Oscillator ODEs via Soft-constrained Physics-informed Neural Network with Small Data. Preprint at <http://arxiv.org/abs/2408.11077> (2024).
- [7] Fang, Q., Mou, X. & Li, S. A physics-informed neural network based on mixed data sampling for solving modified diffusion equations. *Sci. Rep.* **13**, 2491 (2023).
- [8] Mamud, M. L., Mudunuru, M. K., Karra, S. & Ahmmed, B. Quantifying local and global mass balance errors in physics-informed neural networks. *Sci. Rep.* **14**, 15541 (2024).
- [9] Meadows, D. H. *Leverage Points: Places to Intervene in a System*. (The Sustainability Institute, 1999).
- [10] Chattopadhyay, A., Hassanzadeh, P. & Subramanian, D. Data-driven predictions of a multiscale Lorenz 96 chaotic system using machine-learning methods: reservoir computing, artificial neural network, and long short-term memory network. *Nonlin. Processes Geophys.* **27**, 373–389 (2020).
- [11] Wang, S., Sankaran, S. & Perdikaris, P. Respecting causality for training physics-informed neural networks. *Comput. Method Appl. Mech. Eng.* **421**, 116813 (2024).
- [12] Kang, Q. *et al.* Causal prior-embedded physics-informed neural networks and a case study on metformin transport in porous media. *Water Res.* **261**, 121985 (2024).
- [13] Nakamura, Y., Shiratori, S., Nagano, H. & Shimano, K. Physics-Informed Neural Network with Variable Initial Conditions. In Proceedings of the 7th World Congress on Mechanical, Chemical, and Material Engineering (2021). <https://doi.org/10.11159/htff21.113>.
- [14] Finzi, M., Potapczynski, A., Choptuik, M. & Wilson, A. G. A Stable and Scalable Method for Solving Initial Value PDEs with Neural Networks. Preprint at <http://arxiv.org/abs/2304.14994> (2023).

[15] Aldirany, Z., Cottreau, R., Laforest, M. & Prudhomme, S. Multi-level neural networks for accurate solutions of boundary-value problems. *Comput. Method Appl. Mech. Eng.* **419**, 116666 (2024).

[16] Yang, Z. *et al.* Rethinking bias-variance trade-off for generalization of neural networks. Proceedings of the 37th International Conference on Machine Learning, Vienna, Austria, PMLR 119, 2020 <https://proceedings.mlr.press/v119/yang20j/yang20j.pdf> (2020).

[17] Chen, L., Lukasik, M., Jitkrittum, W., You, C. & Kumar, S. It's an Alignment, Not a Trade-off: Revisiting Bias and Variance in Deep Models. Preprint at <http://arxiv.org/abs/2310.09250> (2023).

[18] Psaros, A. F., Meng, X., Zou, Z., Guo, L. & Karniadakis, G. E. Uncertainty quantification in scientific machine learning: Methods, metrics, and comparisons. *J. Comput. Phys.* **477**, 111902 (2023).

[19] Cuong, D. V., Lalić, B., Petrić, M., Nguyen, B. & Roantree, M. Adapting Physics-Informed Neural Networks To Optimize ODEs in Mosquito Population Dynamics. Preprint at <http://arxiv.org/abs/2406.05108> (2024) (*To appear in PLoS ONE journal*).

[20] Petrić, M. *Modelling the influence of meteorological conditions on mosquito vector population dynamics (Diptera, Culicidae)*. PhD thesis, University of Novi Sad, Ghent University (2020).

[21] Vinogradova, E.B. Experimental Investigation of the ecological factors causing diapause of the adults of blood-sucking mosquitos (Diptera, Culicidae) (1960).

[22] Focks, D. A., Haile, D. G., Daniels, E. & Mount, G. A. Dynamic Life Table Model for Aedes aegypti (Diptera: Culicidae): Analysis of the Literature and Model Development. *J. Med. Entomol.* **30**, 1003–1017 (1993).

[23] Erickson, R. A., Presley, S. M., Allen, L. J. S., Long, K. R. & Cox, S. B. A stage-structured, Aedes albopictus population model. *Ecol. Model.* **221**, 1273–1282 (2010).

[24] Cailly, P. *et al.* A climate-driven abundance model to assess mosquito control strategies. *Ecol. Model.* **227**, 7–17 (2012).

[25] Ezanno, P. *et al.* A generic weather-driven model to predict mosquito population dynamics applied to species of Anopheles, Culex and Aedes genera of southern France. *Prev. Vet. Med.* **120**, 39–50 (2015).

[26] Petrić, D., Bellini, R., Scholte, E.-J., Rakotoarivony, L. M. & Schaffner, F. Monitoring population and insecticide resistance of *Aedes albopictus* in Europe. *Parasite. Vector.* **13**, 1–20 (2020).

[27] Raissi, M., Perdikaris, P. & Karniadakis, G. E. Physics-informed neural networks: A deep learning framework for solving forward and inverse problems involving nonlinear partial differential equations. *J. Comput. Phys.* **378**, 686–707 (2019).

[28] Tancik, M., Srinivasan, P., Mildenhall, B., Fridovich-Keil, S., Raghavan, N., Singhal, U., Ramamoorthi, R., Barron, J. & Ng, R. Fourier features let networks learn high frequency functions in low dimensional domains. *Adv. Neural Inf. Process. Syst.* **33**, 7537–7547 https://proceedings.neurips.cc/paper_files/paper/2020/file/55053683268957697aa39fba6f231c68-Paper.pdf (2020).

[29] Wang, S., Wang, H. & Perdikaris, P. On the eigenvector bias of Fourier feature networks: From regression to solving multi-scale PDEs with physics-informed neural networks. *Comput. Method Appl. Mech. Eng.* **384**, 113938 (2021).

[30] Hendrycks, D. & Gimpel, K. Gaussian Error Linear Units (GELUs). Preprint at <http://arxiv.org/abs/1606.08415> (2023).

[31] Kingma, D. P. & Ba, J. Adam: A Method for Stochastic Optimization. Preprint at <http://arxiv.org/abs/1412.6980> (2017).

[32] Paszke, A. *et al.* PyTorch: An Imperative Style, High-Performance Deep Learning Library. Preprint at <http://arxiv.org/abs/1912.01703> (2019).

[33] Loetti, V., Schweigmann, N. & Burroni, N. Development rates, larval survivorship and wing length of *Culex pipiens* (Diptera: Culicidae) at constant temperatures. *J. Nat. Hist.* **45**, 2203–2213 (2011).

[34] Beck-Johnson, L. M. *et al.* The Effect of Temperature on Anopheles Mosquito Population Dynamics and the Potential for Malaria Transmission. *PLoS ONE* **8**, e79276 (2013).

Acknowledgement

This research is supported by the European Union (Grant Agreement No. 101136578). The views and opinions expressed in this publication are solely those of the author(s) and do not necessarily represent the official position of the European Union or the European Commission. Neither the European Union nor the granting authority is responsible for any use that may be made of the information contained herein. Additional support was provided by the Ministry of Science, Technological Development, and Innovation of the Republic of Serbia through two Grant Agreements with the University of Novi Sad, Faculty of Agriculture (No. 451-03-66/2024-03/200117, dated February 5, 2024). This publication also emanates from research partially supported by a grant from Research Ireland (Grant No. SFI/12/RC/2289_P2).

The authors express their gratitude to Dušan Petrić, Aleksandra Ignjatović Ćupina, Mihaela Kavran, Nikola Nožinić and Dragan Dondur for their invaluable efforts in collecting the *Culex pipiens* data used in this study. The data were collected with financial support from the City of Novi Sad, and the VectorNet project (ECDC/EFSA). We would also like to acknowledge the work done within the WNED-X project of the ISIDORe JRA programme, funded by the European Union's Horizon Europe research and innovation programme under grant agreement number 101046133.

Author contributions

BL- design of dynamical systems hybridization concept and main paper writing; DVC-contributed to solution design and development, performed all PINN numerical experiments, contributed to main paper writing; BL and DVC equally contributed to realization of this research; MP- provided meteorological and biological data; MR - contributed to solution design and overall supervision; all authors reviewed the paper.

Competing interests

The author(s) declare no competing interests.

Figure legend

Figure 1 PINN Framework.

Figure 2 Multi-branch Fourier-MLP PINN Framework.

Figure 3 Adult mosquito population simulations (Ab1+Ab2).

Figure 4 Rate of adult mosquito population growth.

Figure SB1 Parameter Sensitivity.

Table legend

Table 1 Performance metrics for Dy_PopMosq and Hy_PopMosq. Values in brackets refer to performance metrics when two worst-performing years are removed.

Table SA1: ODE Model parameters

Table SD1: Annual performance metrics for Dy_PopMosq and Hy_PopMosq

Supplementary A

Parameter	Description	Value	Unit
τ	Temperature		$^{\circ}\text{C}$
γ_{Aem}	Development rate of emerging adults	1.143	days^{-1}
γ_{Ab}	Development rate of bloodseeking adults	0.885	days^{-1}
γ_{Ao}	Ovipositing adult development rate	2	days^{-1}
$f_E (> 0)$	Egg development rate	$0.16 \cdot \left(e^{[0.105(\tau-10)]} - e^{[0.105(38-10) - \frac{1}{5.007}(38-\tau)]} \right)$	days^{-1}
f_P	Pupa development rate	$0.021 \cdot \left(e^{[0.162(\tau-10)]} - e^{[0.162(38-10) - \frac{1}{5.007}(38-\tau)]} \right)$	days^{-1}
f_L	Larva development rate	$f_P \cdot 1.65$	days^{-1}
$f_{Ag} (> 0)$	Development rate of gestating adults	$\frac{\tau - 9.8}{64.4}$	days^{-1}
m_E	Egg mortality rate	$m_E = \mu_E$	days^{-1}
m_L	Larva mortality rate	$\exp\left[-\frac{\tau}{2}\right] + \mu_L$	days^{-1}
m_P	Pupa mortality rate	$\exp\left[-\frac{\tau}{2}\right] + \mu_P$	days^{-1}
$m_A (> \mu_A)$	Mortality rate for A_b	$-0.005941 + 0.002965 \cdot \tau$	days^{-1}
μ_E	Minimum egg mortality rate	0	days^{-1}
μ_L	Minimum larva mortality rate	0.0304	days^{-1}
μ_P	Minimum pupa mortality rate	0.0146	days^{-1}
μ_{em}	Mortality rate during emergence	0.1	days^{-1}
μ_r	Mortality rate during bloodseeking	0.08	days^{-1}
μ_A	Minimum adult mortality rate	1/43	days^{-1}
κ_L	Carrying capacity for larva	$8 \cdot 10^8$	days^{-1}
κ_P	Carrying capacity for pupa	10^7	days^{-1}
σ	Sex ratio at emergence	0.5	-
β	Number of eggs per A_o	$\beta_1 = 141 (np^*), \beta_2 = 80 (p^*)$	-

Table SA1 ODE Model parameters

*np = nulliparous, p = parous

Supplementary B

To assess the most influential parameters in the mosquito dynamical system (equation (1)), we conduct a sensitivity analysis by systematically varying parameters and observing their impact on the system state. We examine 10 parameters: γ_{Aem} , γ_{Ab} , γ_{Ao} , f_E , f_P , f_L , f_{Ag} , m_L , m_P , and m_A , all of which are listed in Table SA1. Each parameter is individually altered at all time points t by -10% , -5% , $+5\%$, and $+10\%$ of its original value, while keeping all other parameters unchanged. The Python ODE Solver is employed to simulate the system under these new conditions. The root mean squared error (RMSE) is then calculated between the new $A_{b1} + A_{b2}$ values and those obtained without parameter changes.

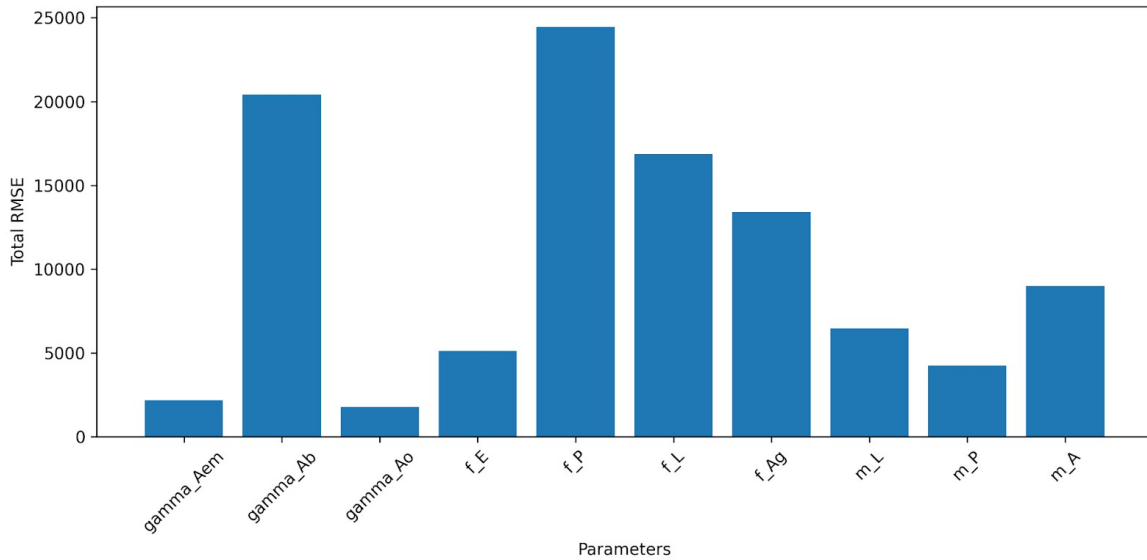


Figure SB1 Parameter Sensitivity.

Figure SB1 illustrates the average RMSE across the four alteration levels for each parameter. The results indicate that the pupa development rate f_P exerts the most significant influence on the adult blood-seeking mosquito population $A_{b1} + A_{b2}$. The development rate of blood-seeking adults f_{Ab} , which directly affects A_{b1} and A_{b2} in the equations, demonstrates slightly less impact. Parameters f_{Ag} and m_A show marginal effects, while other parameters such as γ_{Aem} and γ_{Ao} exhibit minimal influence on the $A_{b1} + A_{b2}$ quantity.

Supplementary C

The experiment begins with the pre-processing of mosquito data and the determination of lower and upper bounds for all data columns, essential for ODE Normalisation. We conduct a simulation using parameters derived from empirical formulas based on climate condition data. The resulting state values from this simulation are used to establish the bounds for the system state. We rescale the collected mosquito counts to align with this range and apply a 5-day window Spline smoothing to mitigate noise in the data. Furthermore, the parameter values obtained from empirical formulas determine their respective ranges while the bounds for climate data are established through their available measurements.

For training using this 2-year dataset, the function A , defined over the time domain, plays a critical role. We train a FourierMLP to interpolate meteorological measurements for any real-valued time t within the domain. This model is configured with 256 Fourier features, followed by three hidden layers, each comprising 128 units. The model outputs two groups of external features: one group consisting of three meteorological variables (temperature, humidity, and precipitation), and another representing the day of the year, with values ranging from 0 to 365.

The neural network architectures are designed as follows: The system state neural network U comprises 256 Fourier features followed by three hidden layers of 128 units each. For the parameter network, we implement a two-branch FourierMLP. The first branch considers 7-day historical meteorological data as input, while the second branch takes day-of-week as input. The second branch takes day-of-week as inputs. This configuration allows the second branch to capture inherent annual patterns of the system, while the former learns the effects of meteorological conditions on mosquito development rates. Both networks employ GELU activation functions for hidden layers and the soft absolute function (equation (7)) to enforce non-negativity.

We train neural network A for 300,000 epochs, saving the checkpoint with the lowest root mean squared error (RMSE). For PINN training, we initially train with only data loss for 10,000 steps, followed by 290,000 steps with the full objective function. PINN checkpoints are saved every 500 steps, and we select the checkpoint yielding the best RMSE when simulating with PINN-learned parameters. The selected checkpoint serves as the final model and is validated using the validation dataset.

We present our results by comparing simulations using PINN-learned parameters against those using baseline parameters, via graphical representations and quantitative metrics. For the PINN-learned simulations, we use the same initial conditions derived from the trained network U for both the training period and the 7-year validation dataset. The baseline simulations use an initial condition of 300 for each state vector component, consistent with the work in (Petric 2020). To facilitate comparison, all simulation results and observations are normalised to the range $[0,1]$ for the calculation of metrics. Our validation metrics include the root mean squared error (RMSE) between $A_{b1} + A_{b2}$, the RMSE of the weekly difference in $A_{b1} + A_{b2}$, and the 7-day 0.2-prominence peak detection recall, precision, and F1-score.

The experiment is implemented in Python, with neural networks and optimisations written in PyTorch. Training is accelerated using a GeForce GTX 4090 GPU. All simulations are executed using

SciPy [S1], using its finite-difference ODE solver [S2]. The peak detection algorithm is also part of the same package.

Supplementary D

Type	Year	RMSE	σ	σ_o	RMSE_rate	σ_rate	σ_o_rate
Hy_PopMosq	2000	0.04	0.04	0.05	0.05	0.02	0.06
	2001	0.21	0.17	0.16	0.25	0.16	0.24
	2002	0.27	0.14	0.22	0.33	0.10	0.29
	2003	0.17	0.13	0.08	0.09	0.08	0.09
	2004	0.10	0.09	0.07	0.09	0.06	0.10
	2005	0.12	0.11	0.15	0.17	0.09	0.15
	2006	0.20	0.09	0.21	0.24	0.07	0.24
	2007	0.32	0.21	0.08	0.16	0.21	0.10
	average	0.18	0.12	0.13	0.17	0.10	0.16
Dy_PopMosq	2000	0.25	0.18	0.05	0.15	0.15	0.06
	2001	0.29	0.15	0.16	0.28	0.13	0.24
	2002	0.28	0.16	0.22	0.32	0.10	0.29
	2003	0.31	0.17	0.08	0.16	0.13	0.09
	2004	0.22	0.15	0.07	0.15	0.09	0.10
	2005	0.22	0.16	0.15	0.19	0.10	0.15
	2006	0.22	0.15	0.21	0.24	0.14	0.24
	2007	0.30	0.16	0.08	0.14	0.09	0.10
	average	0.26	0.16	0.13	0.21	0.12	0.16

Table SD1 Annual performance metrics for Dy_PopMosq and Hy_PopMosq

References Supplementary

[S1] Virtanen, P. et al. SciPy 1.0: Fundamental algorithms for scientific computing in Python. *Nat. Methods* **17**, 261–272 (2020). <https://doi.org/10.1038/s41592-019-0686-2>

[S2] Petzold, L. R. Automatic selection of methods for solving stiff and nonstiff systems of ordinary differential equations. *SIAM J. Sci. Stat. Comput.* **4**, 136–148 (1983). <https://doi.org/10.1137/0904010>